Application of full-waveform inversion to land data: Case studies in onshore Mexico

Cristina Reta-Tang[1], James Sheng[1], Faqi Liu[1], Alfredo Vázquez Cantú[2], and Alejandro Cabrales Vargas[2]

Abstract

Velocity model building and imaging for land surveys are often challenging due to near-surface complexity contaminating the reflection signal. Incorporating full-waveform inversion (FWI) in the velocity model building workflow for land surveys offers benefits not achieved with traditional model building tools, but it also brings difficulties. We have developed an effective model building workflow for land seismic data that incorporates dynamic matching FWI (DMFWI). DMFWI employs an objective function that uses multidimensional local windowed crosscorrelations between the dynamically matched version of observed and synthetic data. Dynamic matching de-emphasizes the impact of amplitudes, allowing the algorithm to focus on using kinematic information for velocity updates. The proposed workflow produces a geologically plausible and consistent model for data acquired with limited offsets. Refraction and reflection tomography may also be included in the workflow. The workflow is applied to onshore surveys in Mexico. Despite challenges of the near-surface geology and limitations of the acquisition parameters in the study areas, the proposed model building workflow successfully derives a high-resolution velocity model that significantly improves the migrated depth image.

Introduction

Full-waveform inversion (FWI) is a robust algorithm that is used to derive velocity models with high resolution and fidelity. It has been widely adopted in the industry. There are many successful examples of its application to marine data, especially for surveys acquired with rich azimuth long offsets and recorded with low-frequency content.

However, building velocity models for land surveys is particularly challenging. Onshore seismic data are acquired on a nonflat datum (topography). This introduces elevation differences between sources and receivers. In addition, the weathering layer (i.e., a layer at or near the surface of mostly heterogenous and unconsolidated low-velocity material) typically results in strong elastic scattering. Vertical geophones register unwanted surface waves known as ground roll that mask P-wave reflections. Resolving the near-surface velocity model is a crucial step in imaging land seismic data. It is traditionally handled by refraction tomography and residual static corrections.

In a few cases, FWI has been incorporated to update the velocity model in the complex near-surface geologies of onshore surveys. Lemaistre et al. (2018) combined first-break picks with Laplace-Fourier FWI. Tang et al. (2021) utilized a workflow that consisted of an alternated source and medium parameter inversion.

Masclet et al. (2021) implemented a novel workflow that demonstrated near-surface characterization by the combined use of first breaks and surface waves. Recently, Leblanc et al. (2022) studied the potential of elastic FWI in a case in the Middle East.

However, applying FWI to land data still presents challenges in many cases. Yilmaz et al. (2022) extensively analyzed the usefulness of FWI to update the near-surface model. Using the vertical component of recorded seismic data, they argued that even elastic inversion, which should better describe land seismic data, is prone to inaccurate P-wave velocity estimations of the near-surface model due to complexities in characteristics of the near surface (e.g., highly heterogeneous, strongly anisotropic, highly attenuating media, etc.). As expected, attempting acoustic inversion to derive the P-velocity model of the near surface often fails because even if the data are limited to the early portion of the shot record, other types of waves (e.g., surface waves and converted modes) are generated in the near surface.

We have developed an effective workflow incorporating FWI to build an accurate velocity model that has been successfully applied to data from many onshore surveys including the two from Mexico discussed in this paper. To minimize the impact of amplitudes, we use multichannel dynamic matching FWI (DMFWI) that promotes the inversion based on kinematic differences and produces more robust results in the presence of strong noise (Mao et al., 2020; Sheng et al., 2020).

The model building workflow is designed to achieve geologically plausible and consistent results for data acquired with limited offsets. In general, the workflow includes the following steps:

- Precondition the input data and denoise to eliminate high-amplitude spikes and strong coherent noise such as ground roll and converted waves. To avoid matching the wrong wave modes, it may be necessary to restrict the type of energy used for inversion by applying properly designed mutes (inner, outer, or both) to the shot gathers.
- Use refraction tomography to build a near-surface model that may be merged with a smooth velocity model reaching maximum depth.
- Use long-wavelength tomographic updates below the near surface to build a global model as the starting model for FWI.
- Apply multiscale DMFWI from low to increasingly higher frequencies using early arrivals, including refractions and wide-angle reflections, to update the shallow portion of the model.
- Apply multiscale reflection DMFWI to invert reflection data for a high-resolution velocity model at deeper depth.

Special Section: Full-waveform inversion

Table 1. Acquisition parameters of the first case study.

Survey number	Bin size (m)	Nominal fold	Maximum offset (m)
1	25 x 25	35	5042
2	30 x 30	80	6742
3	25 x 25	42	6227
4	35 x 35	36	4494
5	30 x 30	286	8209
6	30 x 30	96	6746

It is often necessary and helpful to interleave tomography in the workflow to resolve the long-wavelength model in the deeper portion that cannot be updated by early-arrival FWI. This can accelerate the convergence, especially for data that lack low-frequency signal and have limited offsets.

Methodology

First breaks are picked and used to derive the near-surface model by refraction tomography. The resulting near-surface model will be inserted in a legacy sediment model that is often smooth and lacks details. The first-break picks are also useful for designing proper mutes. This is often necessary so only early arrivals (diving waves and wide-angle reflections) are input to DMFWI to update the shallow model. To prepare the data for DMFWI, minimal processing is applied including spike editing, ground-roll noise attenuation, and residual statics correction. The velocity model is calibrated using check-shot information and updated by global reflection tomography. Anisotropy parameters are derived using focusing analysis (Cai et al., 2009). The resulting velocity and anisotropy models are used as the starting point for DMFWI.
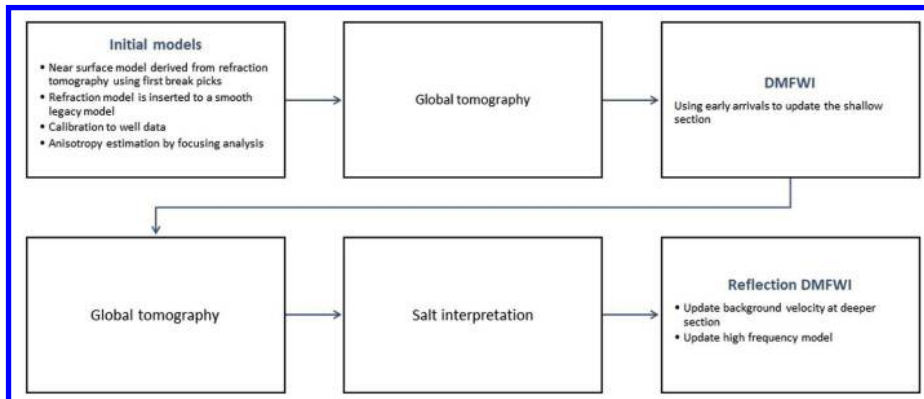
It is well known that FWI is a highly nonlinear inversion algorithm aimed at producing a velocity model that best explains the field data. This iterative algorithm involves forward modeling and migration of data residuals. The iteration stops when the synthetic shots get close enough to the real data. Then, it is assumed that the resulting velocity model is a good estimate of the true model.

The DMFWI algorithm employs an objective function that maximizes multidimensional crosscorrelation between the dynamically matched synthetic and observed data in local windows (Mao et al., 2020). The window used in DMFWI is localized in time and space. This gives more reliable measurements of the correlations between input and synthetic data and allows it to focus on kinematic information. DMFWI is a multiscale algorithm in which the window size is defined by the frequency band in the iterative process. The multichannel algorithm mitigates the influence of noise in the input data, overcoming

Figure 1. Model building workflow.

Figure 2. Model overlaid on the Kirchhoff PSDM image (left), Kirchhoff PSDM image (middle), and migration gathers (right) for the initial model (top row) and DMFWI model (bottom row). The red arrows indicate image improvements.
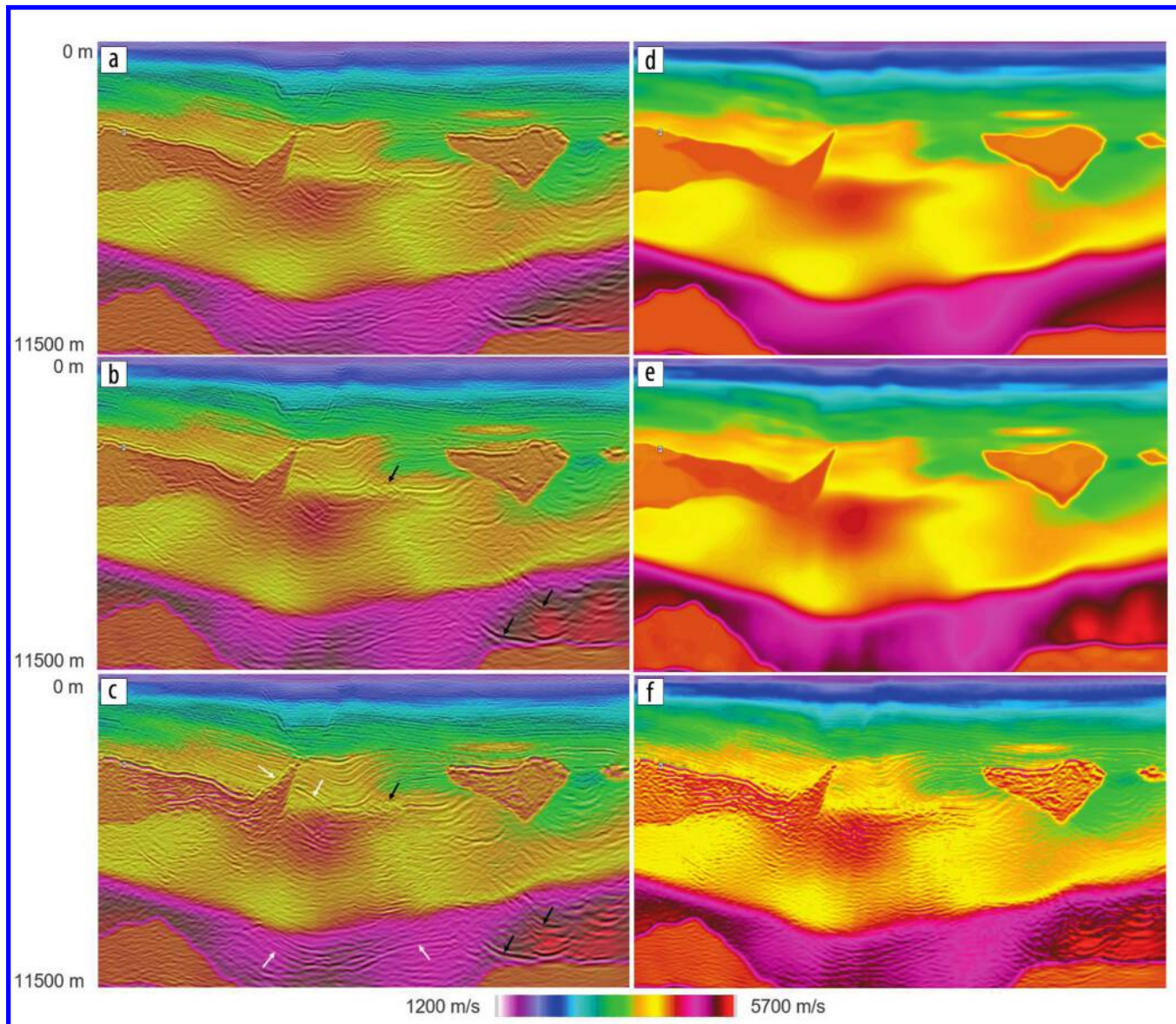
Figure 3. (a) The 25 Hz RTM overlaid with the velocity model before reflection DMFWI as shown in (d). (b) The 25 Hz RTM overlaid with the velocity model after first-pass reflection DMFWI as shown in (e). (c) The 25 Hz RTM overlaid with the velocity model after final reflection DMFWI as shown in (f). Black and white arrows show image improvements using the DMFWI velocity model after the first-pass reflection DMFWI and final reflection DMFWI, respectively.

poor signal-to-noise (S/N) ratio. Throughout this workflow, DMFWI uses all of the information in the data including reflections and refractions. This allows reduced cycle skipping and obtains reliable velocity updates for surveys that are less optimal to the algorithm (e.g., limited offsets, missing low-frequency signal, high noise contamination, etc).

First case study

The first example includes data from six surveys that were acquired mostly using dynamite sources. Only a limited number of shots were acquired using vibroseis. As shown in Table 1, the acquisition parameters are significantly different between surveys. The maximum offsets vary between 4494 and 8209 m. Only a small portion of the surveys (less than 25%) was acquired with the maximum offset of 8209 m. This imposes limitations to the penetration of diving waves in most areas. The noise in the data

Table 2. Acquisition parameters of the second case study.

Survey number	Bin size (m)	Nominal fold	Maximum offset (m)
1	40 x 40	36	5723
2	35 x 50	36	5318
3	40 x 40	36	5723
4	25 x 25	36	6550
5	25 x 25	36	5496
6	25 x 25	36	5496

also limits the minimum usable frequency for FWI to 5 Hz. The model building workflow implemented in this case study, (Table 1) includes DMFWI using early arrivals to update the shallow section and reflection data for deeper target. This generates background velocity and high-frequency updates. In this test, only
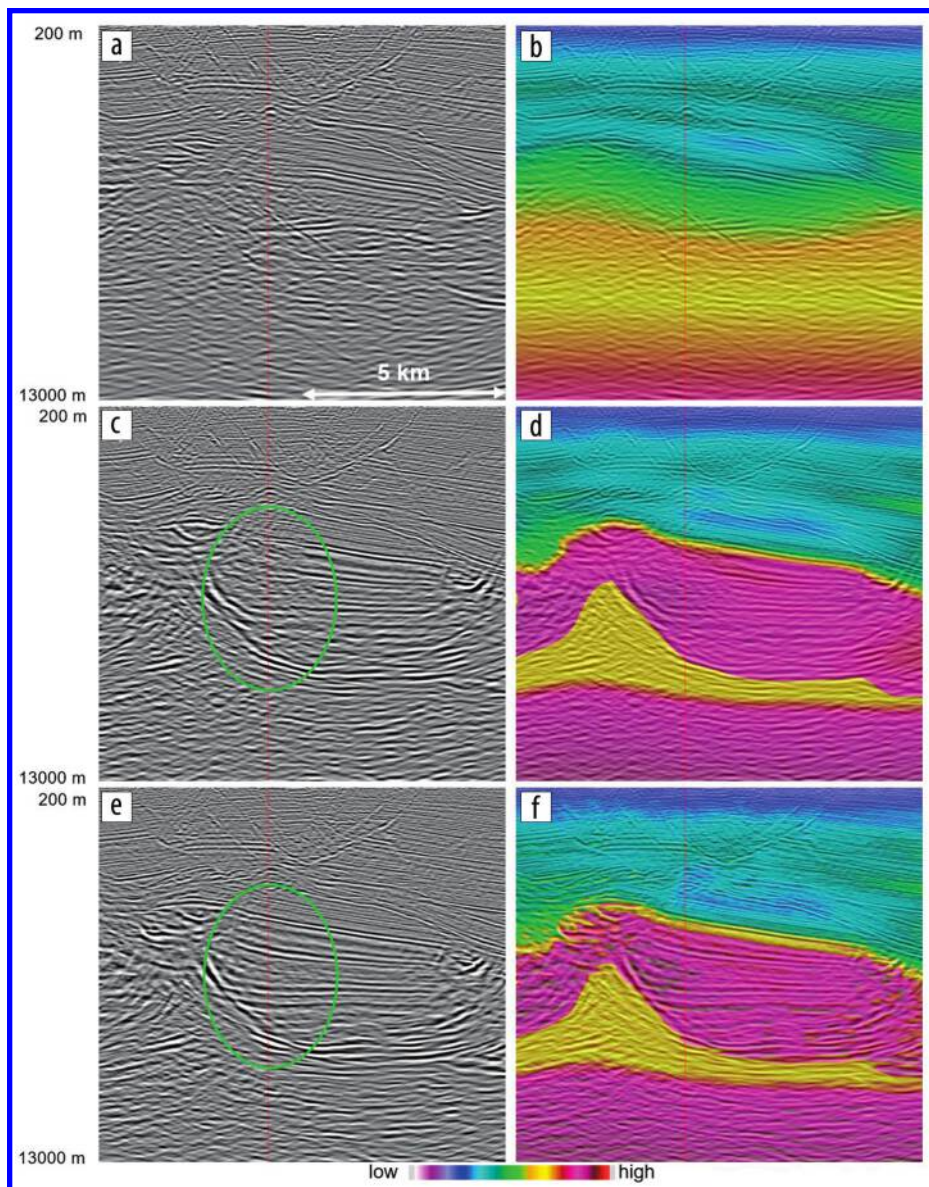
Figure 4. (a) One inline of the RTM image using the initial model before the model building workflow. (b) The velocity model overlaid with the corresponding RTM image. (c) Inline of the RTM image using the velocity model after the first pass of DMFWI. (d) Overlay of the first-pass DMFWI model with the corresponding RTM image. (e) Inline of the RTM image using the final reflection DMFWI model. (f) Overlay of the final DMFWI model with the corresponding RTM image.

shallow update (bottom row). The complex faulting above the salt body in conjunction with the limited offsets produces low-quality picks for tomography and yields unresolved velocity features. Furthermore, the resolution of the tomographic velocity is insufficient to impact the image in the faulted area. Improvement of the tomographic results would require editing to the velocity perturbation in a target-oriented fashion. This is time consuming and not always practical in large projects. On the contrary, DMFWI automatically updates the remaining velocity errors in areas of low-quality gathers. The velocity model after DMFWI has better-focused migrated events above the salt body. Fault planes are better defined on the image, and the gathers are flatter.

Following the shallow update using diving-wave FWI, the workflow moves to update the deep section using reflection FWI. Due to the limited offsets of acquisition, the background velocity for the mid to deep section is built as accurately as possible before running reflection DMFWI. The workflow includes additional passes of multiazimuth tomography and interpretation of allochthonous salt bodies, carbonates, and autochthonous salt. We then run two passes of reflection DMFWI using the fully processed data, which have designature and zero phasing applied. The long-wavelength statics have been removed, and residual statics have been applied. A zero-phase wavelet was estimated for each survey from the spectrum of the corresponding input

data collected using a dynamite source are used for DMFWI due to a very limited number of available vibroseis shots (less than 1%). The shots are first muted to limit the energy to early arrivals (diving waves and wide-angle reflections). DMFWI is run with increasingly higher frequency bands up to a maximum frequency of 15 Hz. Minimum phase wavelets are extracted from the data for the DMFWI workflow. We use a finite-difference method with low velocity and low-density padding above the topography to generate acoustic synthetic data (Sheng et al., 2022).

The starting model uses near-surface velocity obtained from refraction tomography. The deeper part is a smoothed version of a legacy model followed by one pass of global tomography. Figure 2 shows the model overlaid on a Kirchhoff prestack depth migration image, Kirchhoff image, and migration gathers, respectively, for the initial model (top row) and the DMFWI model for the

data. The first pass of reflection FWI is run up to 12 Hz and updates the velocities using mainly the wave path or tomographic kernel. Figure 3a shows a 25 Hz reverse time migration (RTM) image overlaid with the model before the FWI update shown in Figure 3d. This is the starting model for reflection FWI. Figure 3b shows the 25 Hz RTM image overlaid with the model after the first pass of reflection FWI displayed in Figure 3e. As pointed to by the black arrows, this pass of reflection FWI provides additional uplift to the mid and deeper portion of the image, but it mainly corrects for the background velocity. Finally, we run high-frequency reflection DMFWI up to 25 Hz to obtain a high-resolution velocity model to 12 km depth (Figure 3f). As pointed to by the white arrows, this model provides a significant improvement of the image. Figure 3c shows the image section overlaid with the model after the final reflection FWI.

Second case study

The second data set is a merge of six surveys acquired mainly with a dynamite source and a reduced number of vibroseis shots. The maximum offset varies between 5318 and 6550 m (see Table 2 for a summary of the main acquisition parameters). The main area of interest is mostly covered by a survey with approximately 5496 m of maximum offset. The sedimentary model at the target level consists of platform carbonate rocks. The study area presents a structural high generated by the evacuation of salt. The potential targets are dipping carbonates of a few hundred meters in thickness located below Tertiary salt. The allochthonous salt extends upward, cutting the formations of interest (Sheng et al., 2022).

A similar model building workflow has been applied to this data as the one described in the previous example. The initial model was built by inserting a near-surface model derived from refraction tomography into a smoothed legacy model. Figures 4a and 4b show one inline of the RTM image migrated with the initial model and the same image overlaid with the initial velocity. Figures 5a and 5b show one crossline of the RTM image with and without overlaying the model, respectively. The model building workflow includes DMFWI to update the shallow section using early arrivals (diving waves and wide-angle reflections), passes of global tomography, salt interpretation, carbonate interpretation, and carbonate tomography for deep background velocity updates. The same inline of the RTM image migrated with the updated model with and without velocity overlay is shown in Figures 4c and 4d, respectively. Figures 5c and 5d show the corresponding crossline images. Finally, we run high-frequency reflection DMFWI, starting from 12 Hz and gradually increasing the frequency up to 30 Hz, to obtain a high-resolution velocity model. RTM images using the final high-frequency FWI velocity with and without velocity overlay are shown in Figures 4e and 4f, respectively. Figures 5e and 5f show the crossline images. Clearly, RTM using the final DMFWI model (Figures 4e, 4f, 5e, and 5f) shows significantly better definition of the carbonate layer and sediment packages above the top of the carbonate layer. The events below this layer also become more continuous. Areas of improvement are marked with green circles and arrows in Figures 4 and 5. Figure 6 shows a depth slice at 3300 m of the initial model, the model after refraction tomography and
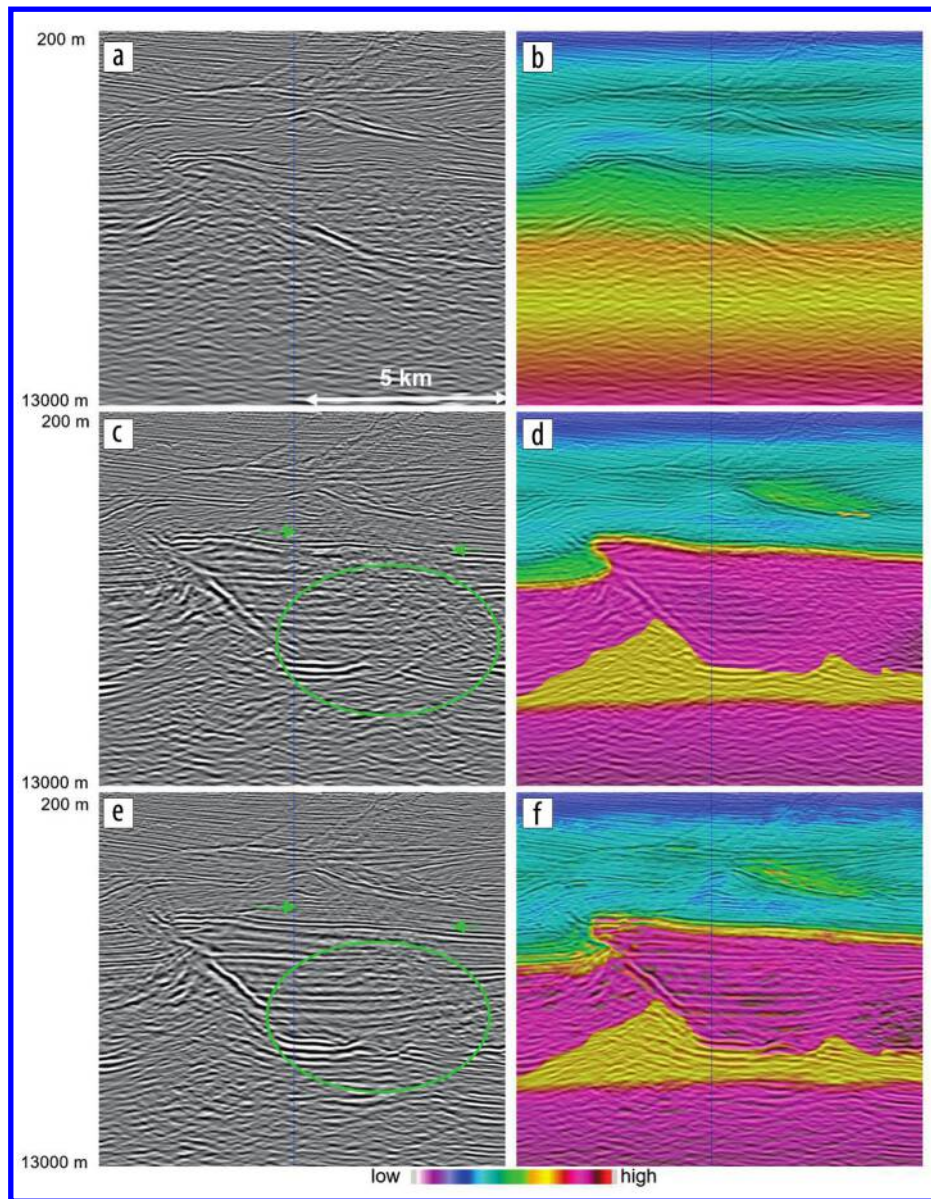
Figure 5. (a) One crossline of the RTM image using the initial model before the model building workflow. (b) The velocity model overlaid with the corresponding RTM image. (c) Crossline of the RTM image using the velocity model after the first pass of DMFWI. (d) Overlay of the first-pass DMFWI model with the corresponding RTM image. (e) Crossline of the RTM image using the final reflection DMFWI model. (f) Overlay of the final DMFWI model with the corresponding RTM image.

diving-wave DMFWI, and the final reflection FWI model. Slides at the same depth of the corresponding RTM images are shown in Figures 6d–6f. The sequence in the figures clearly shows the improvement in the image using the velocity model at the different stages of the workflow.

Conclusions

DMFWI has been integrated successfully into a model building workflow for land data. The algorithm's ability to dynamically match the observed and predicted data helps reduce the impact of relatively low S/N for model building. Despite the challenges and limitations of the acquisition parameters of the surveys in the study areas discussed in this paper, the workflow has proven to be robust for land data, yielding a high-resolution velocity model. DMFWI improves the accuracy and resolution

of the velocity model. This has resulted in significant uplift of the image quality in the two land examples. **TLE**

Acknowledgments

Data and materials availability

Data associated with this research are confidential and cannot be released.

Corresponding author: faqi.liu@tgs.com

References

Cai, J., Y. He, Z. Li, B. Wang, and M. Guo, 2009, TTI/VTI anisotropy estimation by focusing analysis, Part I: Theory: 79th Annual International Meeting, SEG, Expanded Abstracts, 301–305, https://doi.org/10.1190/1.3255480.

Leblanc, O., A. Sedova, G. Lambaré, T. Allemand, O. Herman, D. Carotti, D. Donno, and N. Masmoudi, 2022, Elastic land full-waveform inversion in the Middle East: Method and applications: 83rd Annual Conference and Exhibition, EAGE, Extended Abstracts, https://doi.org/10.3997/2214-4609.202210375.

Lemaistre, L., J. Brunellière, F. Studer, and C. Rivera, 2018, FWI on land seismic datasets with topography variations: Do we still need to pick first arrivals?: 88th Annual International Meeting, SEG, Expanded Abstracts, 1078–1082, https://doi.org/10.1190/segam2018-2995924.1.

Mao, J., J. Sheng, Y. Huang, F. Hao, and F. Liu, 2020, Multi-channel dynamic matching full-waveform inversion: 90th Annual International Meeting, SEG, Expanded Abstracts, 666–670, https://doi.org/10.1190/segam2020-3427610.1.

Masclet, S., G. Bouquard, and H. Prigent, 2021, Multi-wave and full-waveform inversion in southern Oman: 82nd Conference and Exhibition, EAGE, Extended Abstracts, https://doi.org/10.3997/2214-4609.202010731.

Sheng, J., J. Mao, F. Liu, and M. Hart, 2020, A robust phase-only reflection full waveform inversion with multi-channel local correlation: 81st Conference and Exhibition, EAGE, Extended Abstracts, https://doi.org/10.3997/2214-4609.202012012.

Sheng, J., C. Reta-Tang, F. Liu, A. Vázquez Cantú, and A. Cabrales Vargas, 2022, Full-waveform inversion and FWI imaging for land data: Second International Meeting for Applied Geoscience and Energy, SEG/AAPG, Expanded Abstracts, 827–831, https://doi.org/10.1190/image2022-3749887.1.

Tang, Y., D. Gaines, J. Hefti, S. Every, E. Neumann, and R. Pharis, 2021, Land full-wavefield inversion for addressing complex near-surface challenges in the Delaware Basin: First International Meeting for Applied Geoscience and Energy, SEG/AAPG, Expanded Abstracts, 702–706, https://doi.org/10.1190/segam2021-3594001.1.

Yilmaz, Ö., K. Gao, M. Delic, J. Xia, L. Huang, H. Jodeiri, and A. Pugin, 2022, A reality check on full-wave inversion applied to land seismic data for near-surface modeling: The Leading Edge, **41**, no. 1, 40–46, https://doi.org/10.1190/tle41010040.1.
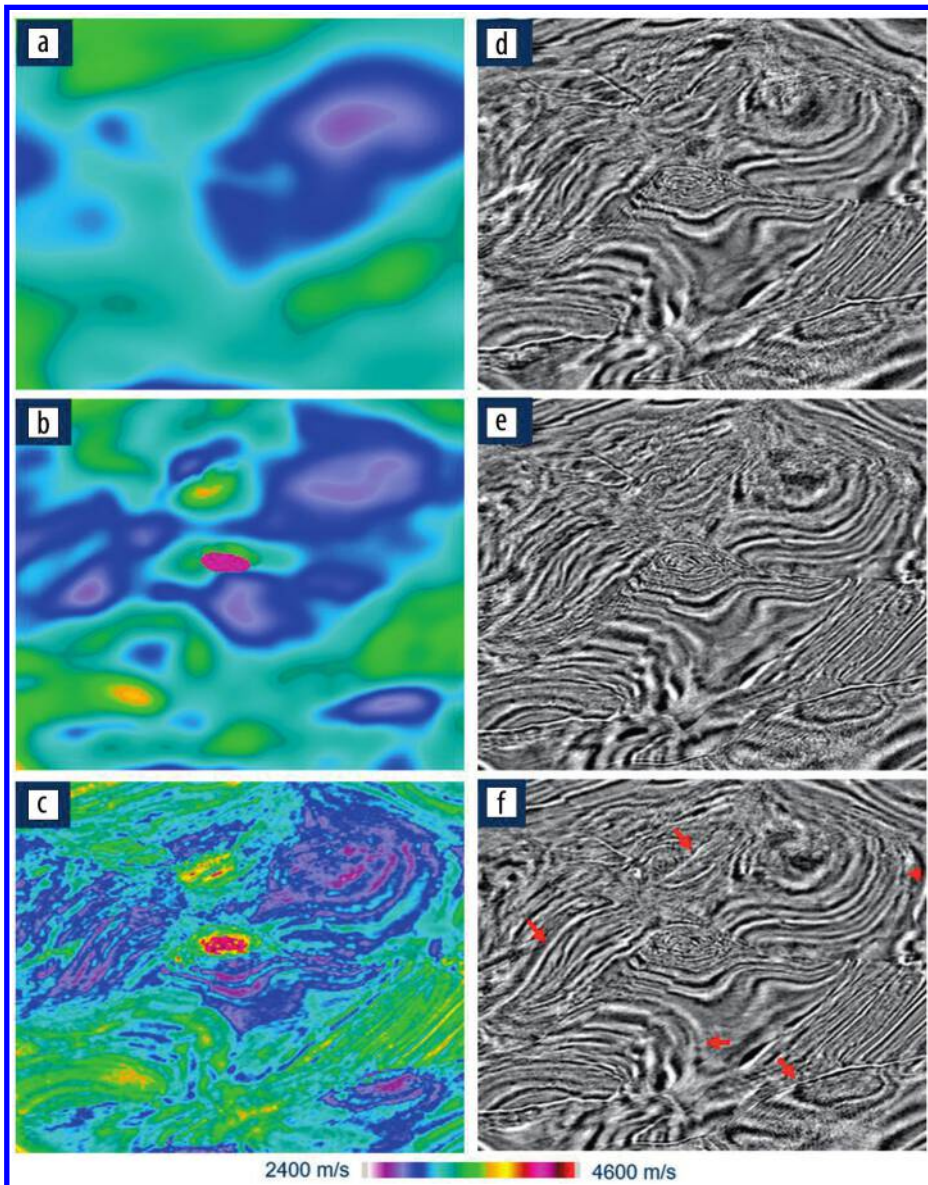
Figure 6. Depth slices at 3300 m for (a) the initial model, (b) model after refraction tomography and diving-wave DMFWI, (c) model after reflection FWI, (d) RTM image corresponding to the initial model in (a), (e) RTM image migrated with the model after refraction tomography and diving-wave DMFWI in (b), and (f) RTM image using the model after reflection FWI in (c).